Thin Solid Films 635 (2017) 66–72

Contents lists available at ScienceDirect

Thin Solid Films

journal homepage: www.elsevier.com/locate/tsf

Textured and micropillar silicon heterojunction solar cells with hot-wire deposited passivation layers

L.W. Veldhuizen [a,*], W.J.C. Vijselaar [b], H.A. Gatz [a], J. Huskens [b], R.E.I. Schropp [a]

[a] Eindhoven University of Technology (TU/e), Department of Applied Physics, Plasma & Materials Processing, P.O. Box 513, 5600 MB Eindhoven, The Netherlands
[b] University of Twente, MESA + Institute for Nanotechnology, Molecular NanoFabrication, P.O. Box 217, 7500 AE Enschede, The Netherlands

ARTICLE INFO

Article history:
Received 30 September 2016
Received in revised form 20 February 2017
Accepted 20 February 2017
Available online 10 March 2017

Keywords:
Solar cells
Silicon heterojunction
Hot wire chemical vapor deposition
Micropillar arrays

ABSTRACT

The passivating quality of hydrogenated amorphous silicon thin films is essential for achieving high open-circuit voltages in silicon heterojunction solar cells. This work reports our progress towards the use of hot wire chemical vapor deposition for fabricating these passivation layers. We have achieved 19.4% energy conversion efficiency for a solar cell with a conventional alkali-etched pyramidal texture. Next, we tested radial heterojunction devices that consist of up to 20-μm high micropillar arrays. Proper passivation of these devices is challenging, since the structures feature an enlarged surface area and vertical walls. We have made use of the ability of hot wire chemical vapor deposition to deposit conformal thin films at high deposition rate. The micropillar solar cells show only limited reduction of open-circuit voltage in comparison to a flat reference solar cell and have an improved overall performance. We created additional stacked multijunction silicon-based junctions on top of the micropillars to increase the open-circuit voltage of the solar cells for future applications in which a higher potential is required such as water splitting devices.

1. Introduction

The highest solar cell efficiencies using crystalline silicon are obtained for cells employing the silicon-heterojunction (SHJ) concept [1]. These cells benefit from excellent passivation of interface defects at the surfaces of crystalline Si wafers. Commonly, hydrogenated amorphous silicon (a-Si:H) is used to render the surface dangling bonds of the wafers electrically inactive by saturating these bonds with atomic hydrogen that is present in ultra-thin films of such materials. These films have to be very thin (~4 nm) and conformal as they bring about parasitic absorption. Plasma enhanced chemical vapor deposition (PECVD) is the most common method for the fabrication of a-Si:H for SHJ devices, hence the majority of the research on this topic has focusing on this method. Despite the high performance obtained worldwide for SHJ cells with PECVD a-Si:H [1–4], hot wire chemical vapor deposition (HWCVD) is an interesting alternative method for the deposition of the a-Si:H films. This method offers various advantages over PECVD such as a high concentration of hydrogen radicals at the surface available for passivation [5]. Due to the almost complete absence of ions or electric field, there is improved conformality at high deposition rates and no risk of ion bombardment damage to the wafer interfaces [6]. Additionally, HWCVD is a suitable in-line deposition technique and can lead to lower cost-of-ownership in the mass fabrication of SHJ cells [7].

We have developed a HWCVD process for thin, highly passivating a-Si:H layers on n-type crystalline silicon (c-Si) wafers. These layers are suitable to be used with p-type nanocrystalline silicon oxide (nc SiO_x:H) layers that feature better optical transmission than conventional a-Si:H p-type emitter layers. We have applied our process to fabricate SHJ solar cells with a random pyramid texture and cells with a micropillar front texture. The micropillar or microwire concept is widely considered for photovoltaic applications due to its potential for enhanced absorption and/or carrier collection [8–10]. Micropillar solar cells are not only considered for solar electricity but also for the production of solar fuels by means of photoelectrochemical water splitting as they feature a large reaction surface [11]. To passivate the c-Si surface of the pillars in our study, that have vertical walls up to 20 μm high, we fully exploit the capabilty of HWCVD to create conformal layers. To boost the operating voltage of our devices we added extra amorphous silicon-based radial junctions on top of the SHJ solar cells, to achieve voltages that are high enough for photoelectrochemical water splitting.

2. Experimental details

2.1. SHJ fabrication

All silicon thin films were deposited in a multi-chamber system that consists of separate reactors for n-type, p-type, and intrinsic silicon films to avoid cross-contamination. The intrinsic films were deposited by HWCVD at a rate of ~0.4 nm/s using two heated (1700 °C) parallel

* Corresponding author.
E-mail address: l.w.veldhuizen@tue.nl (L.W. Veldhuizen).

http://dx.doi.org/10.1016/j.tsf.2017.02.048
0040-6090/

0.3-mm tantalum filaments at a distance of 35 mm from the substrate. Fig. 1 shows a top view of the opened reactor. Further details about this process can be found elsewhere [12]. The doped layers were deposited by 13.56 MHz PECVD at a low rate of <0.1 nm/s to promote conformal deposition. The n-type c-Si wafers in this study were cleaned for 2 min in a 1% HF solution. The dangling bonds on both sides of the c-Si surface were passivated with a-Si:H passivation layers with a thickness of 4 nm, deposited at a temperature of 130 °C. These a-Si:H layers were made at a process pressure of 2 Pa, using undiluted silane as precursor gas. An a-Si:H n-type back surface field (BSF) layer of 20 nm was deposited at a temperature of 200 °C on the rear side of the solar cell. On the other side, a triple-layer p-type emitter was deposited at a temperature of 160 °C. The core of this emitter consisted of a 10-nm thick hydrogenated nc-SiO_x:H p-layer [13]. This material has a higher optical band gap ($E_g = 2.3$ eV) and a considerably lower refractive index at a photon energy of 2 eV ($n(2\text{ eV}) = 2.7$) compared a non-oxide film ($E_g = 2.1$ eV, $n(2\text{ eV}) = 3.8$). Whereas the oxygen in this layer opens up the band gap, making the layer more transparent, it also delays the formation of crystallites that are desired for efficient doping and sufficient conductivity. The layer is therefore preceded by 5 nm of nc-Si:H (p) to provide an early onset of crystallization. The top of the stack is a highly conducting 3-nm thick nc-Si:H p-layer that can form an Ohmic contact with the transparent indium tin oxide (ITO) front electrode. The ITO front electrodes were 80 nm thick and deposited by magnetron sputtering on the front and rear side. All solar cells were completed with thermally evaporated layers of 300-nm thick Ag back contacts and front contact grids.

2.2. Texturing

Silicon heterojunction cells were fabricated on pyramidal texture and on micropillar arrays. The pyramidal texture was fabricated using 160-μm thick n-type silicon Czochralski wafer with ⟨100⟩ orientation as the base material. The texture etch was a conventional random-pyramid texture on both sides, created with a (isopropanol-free) KOH chemical etch. Instead of the smoothening treatment that is often done for SHJ wafers to reduce the risk of localized recombinative paths situated at the pyramid valleys [14,15], only an HNO_3 cleaning etch treatment was used which did not alter the pyramidal texture. This leaves a less smooth surface than using a full smoothening treatment. The solar cells have an active area of 0.69 cm^2. After fabrication, the cells were annealed in a nitrogen atmosphere at 190 °C for 3 h.

Arrays of 4-μm diameter silicon micropillars with various lengths and spacings were fabricated by growing a hard mask of 200 nm silicon dioxide (SiO_2) on the n-type c-Si wafer using wet oxidation at 1100 °C for 30 min [10]. By means of standard UV-lithography, the pattern of the pillar arrays was defined in photoresist (Olin 907-17), and post-baked for 10 min at 120 °C after exposure and development. Subsequently, this pattern was transferred into the SiO_2 by reactive-ion etching (Adixen DE). Although both the SiO_2 and photoresist layer acted as mask during cryogenic deep reactive-ion etching (DRIE) of the micropillars, the SiO_2 is more resilient to the DRIE process and therefore enables better defined micropillar features. The micropillars were etched via cryogenic (−100 °C) deep reactive ion etching (DRIE; Adixen MS100SE, 1000 W) of silicon, using sulfur hexafluoride (SF_6, 200 sccm) for etching silicon and O_2 (30 sccm) for passivating the sidewalls. After etching, the remaining photoresist and SiO_2 was removed via oxygen plasma (Tepla360) and BHF, respectively. Fig. 2(a) schematically shows the fabrication process of the micropillar arrays and (b) shows a side view scanning electron microscopy (SEM) image of ~20-μm long micropillars.

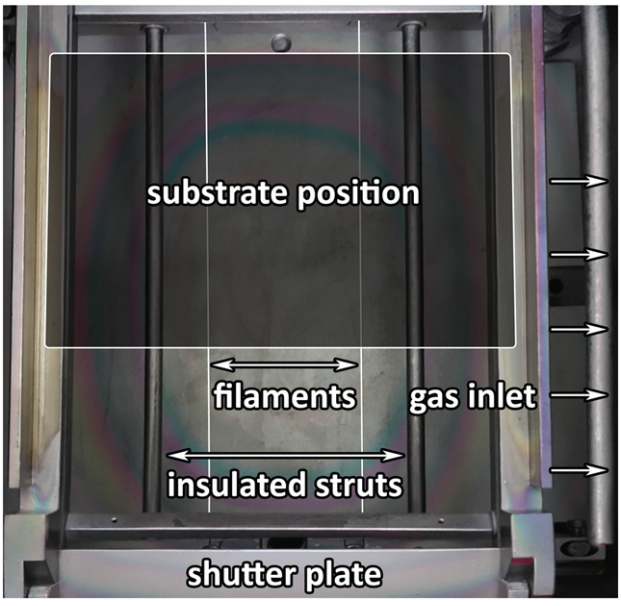

Fig. 1. Top view of the opened HWCVD reactor. Two tantalum filaments span the reactor interior. Insulated spacers are used to tension the filaments. The rectangle indicates the position of the sample in a sample holder which is located 35 mm above the filaments. A shutter plate is slid between the filaments and the sample to prevent film growth during the initiation and completion of the deposition process.

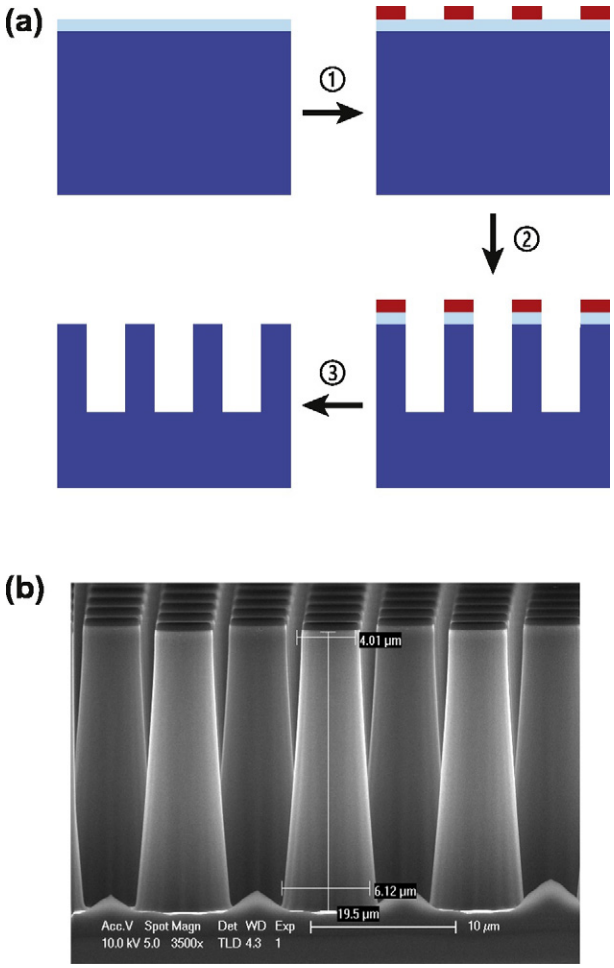

Fig. 2. (a) Schematic cross sections of a c-Si wafer during the micropillar fabrication process. ① A photoresist pattern was applied on a c-Si (n) wafer with a 200-nm thick SiO_2 layer using UV-lithography. ② The pattern was transferred into the SiO_2 layer by reactive-ion etching and subsequently into the wafer by cryogenic deep reactive-ion etching. ③ The photoresist and SiO_2 layers were removed by oxygen plasma treatment. (b) Scanning electron microscopy (SEM) image showing ~20-μm-long micropillars, directly after fabrication and before removal of the mask.

2.3. Micropillar SHJ cells fabrication

SHJ solar cells were created on these micropillar arrays using the same layer stack as for the random pyramid texture. The cell area of these solar cells was reduced to an active area of 0.13 cm^2 to allow for a higher quantity of pillar variations within the same deposition run. A schematic cross section of the micropillar-based SHJ device is shown in Fig. 3(a).

2.4. Micropillar a-Si:H/SHJ tandem cells fabrication

For tandem solar cells, a 20-nm phosphorus-doped nc-Si:H n-type layer was grown on top of the nc-Si(O):H (p) emitter of a SHJ cell. Together, these layers form the tunnel recombination junction (TRJ) that is needed for a proper connection between the two sub-cells. The individual layers of the TRJ have low dark current activation energies ($E_a = 0.009$ eV and 0.011 eV for the nc-Si:H n-type and p-type layer, respectively), which facilitates high tunneling efficiency [16]. As absorber layer, a 350-nm thick a-Si:H intrinsic HWCVD layer with a band gap of 1.86 eV was fabricated. This intrinsic film was deposited in a similar manner as the a-Si:H passivation layers of the SHJ devices, except at an increased substrate temperature of 270 °C. On top of this absorber layer, a nc-Si(O):H (p) emitter was grown as previously described. Thin (<3 nm) PECVD intrinsic a-Si:H buffer layers were introduced at the i/n and i/p interface in order to improve the contact between these layers. This process is described elsewhere [17]. A schematic representation of such a device is given in Fig. 3(b).

2.5. Micropillar a-Si:H/a-SiGe:H/SHJ triple cells fabrication

For triple junction solar cells, we used the previously discussed SHJ structure and created a 20-nm phosphorus-doped nc-Si:H n-type layer on top of the nc-Si(O):H (p) emitter to form a TRJ. A hydrogenated amorphous silicon germanium (a-SiGe:H) layer of 120 nm was deposited with HWCVD as a middle cell absorber. The band gap of this layer was graded to facilitate the extraction of photo-generated charge carriers. The band gap was varied from 1.86 eV to 1.37 eV and back by varying the germanium content as described elsewhere [18]. The material with the lowest band gap was 60 nm thick and positioned 15 nm from the front interface. At the rear side of the film, a 45-nm thick graded-band gap layer was used. On top of the a-SiGe:H layer, a nc-Si:H (p)/nc-Si:H (n) stack was added to construct a second TRJ between the top (a-Si:H) and middle cell (a-SiGe:H). As top cell, a 350 nm intrinsic a-Si:H was grown with a 20 nm nc-Si(O):H p-type layer. Again, thin PECVD buffer layers were used at the i/n and i/p interfaces of the middle and top cell. A schematic representation is given in Fig. 3(c).

2.6. Electrical characterization

The current density-voltage (J–V) characteristics of the solar cells in this study were measured at 25 °C under a WACOM dual source solar simulator (class AAA) calibrated to the AM1.5G spectrum. A shadow mask was used to prevent current collection from outside the active area of the cells. The current densities are presented with respect to the active area of the solar cells (the area that is not covered by the contact grid). The external quantum efficiency (EQE) was measured under short-circuit conditions in the range of 290–1200 nm using a xenon lamp and a monochromator. The EQE of the multijunction devices was acquired using colored LED bias light to measure the response of the sub-cells separately by saturating the photocurrent of the other sub-cell(s).

2.7. Imaging

The devices were imaged with a Nova 600 Dual Beam, high resolution scanning electron microscopy (SEM)/focused ion beam (FIB) setup. A Ga^+ liquid metal ion source was used to mill away approximately half of a single pillar, along the pillar length with respect to the footprint of each array, with a beam current of 0.92 nA and a 30 kV extraction voltage.

3. Results and discussion

3.1. Random textured SHJ cells

For the cells on pyramidal texture, the J–V characteristics showed a strong "S-shape" behavior before annealing, which is an indication of a low amount of active doping centers in the p-layers [19]. Fig. 4 shows both the J–V and EQE characteristics of the best performing solar cell after the annealing treatment. The energy conversion efficiency (η) of this solar cell exceeds that of all previously reported efforts in which HWCVD was used as deposition method for the passivation layers in a similar structure [19,20]. The J–V characteristics were scaled, to match the short circuit current density (J_{sc}) value that is extracted from the EQE measurements which was only 5% lower than the J_{sc} value as measured with the solar simulator. The average open-circuit voltage (V_{oc}) of the best five cells was 704 mV, which is exemplary for the excellent passivation capabilities of the 4-nm thick a-Si:H passivation layer. The V_{oc} is known to increase for larger solar cell areas due to a relative reduction of the resistive load imposed by the dark perimeter of the cell. This was reflected by a ~20-mV V_{oc} increase upon removal of the shadow mask.

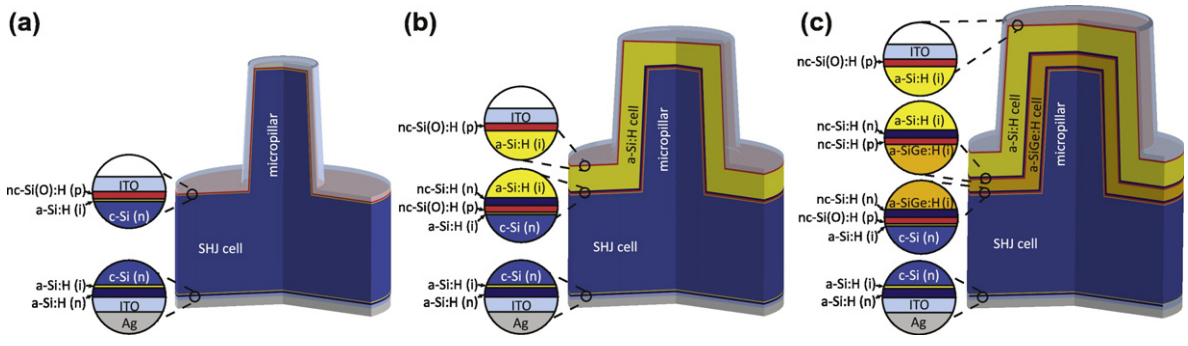

Fig. 3. Schematic cross-section of a micropillar-array (a) SHJ cell solar cells, (b) a-Si:H/SHJ tandem solar cell, and (c) a-Si:H/a-SiGe:H/SHJ triple junction solar cell. The dimensions of the wafer and micropillar are not to scale. Insets show the composition of the thin films that are used in the design. The nc-Si(O):H (p) layers consists of a nc-SiO_x:H film that is sandwiched between two nc-Si:H (p) layers. The a-SiGe:H sub-cell uses a single nc-Si:H p-type layer for its high conductivity. Ag contact grids (not shown) are used as front electrode. The thin PECVD buffer layers in the tandem and triple junction cells are not shown. For the SHJ cells with random pyramid texture the same layer stack was used as in (a).

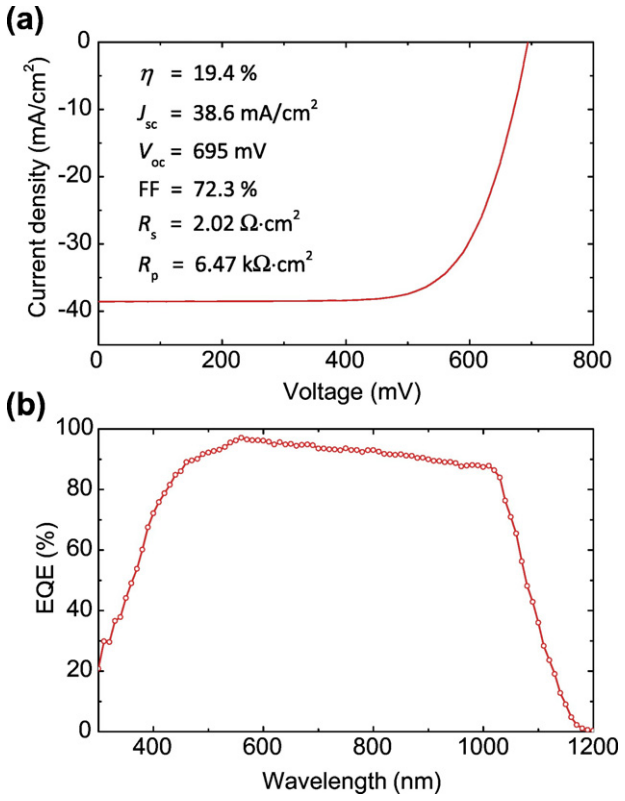

Fig. 4. Results of a typical SHJ solar cell with a-Si:H passivation layers deposited by HWCVD. (a) Current density-voltage characteristic and (b) External quantum efficiency. The series resistance (R_s) and the parallel or shunt resistance (R_p) were derived from the tangent to the current density at the V_{oc} and J_{sc} positions, respectively.

3.2. Micropillar SHJ cells

We continued by testing the capabilities of HWCVD to passivate silicon wafers with more extreme morphologies. To this end we fabricated heterojunction solar cells with several types of micropillar arrays on its front-facing side. Fig. 5 gives an overview of 20 μm long micropillars with three different hexagonal pitches (i.e. 8 μm, 10 μm, and 15 μm pitch, respectively). Each of these micropillars has a heterojunction solar cell grown conformally over the micropillars as described in the experimental details section.

Table 1 shows the electrical characteristics of the SHJ solar cells as compared to a simultaneously fabricated flat cell. The J_{sc}, as determined by EQE measurements, increased upon introducing the micropillars due to geometric light trapping and/or better current collection. Interestingly, a larger inter-pillar spacing distance also benefitted the J_{sc} value. This

Table 1
Results of SHJ solar cells with a micropillar front texture with different spacings compared to that of a flat reference cell. The length of the micropillars was 20 μm.

Spacing (μm)	V_{oc} (mV)	J_{sc} (mA/cm²)	FF (%)	η (%)	R_s (Ω·cm²)	R_p (kΩ·cm²)
Flat	648	33.85	71.4	15.66	2.14	5.24
8	628	33.90	73.8	15.70	1.53	1.53
10	627	34.56	74.0	16.05	1.61	2.75
15	632	34.93	75.1	16.59	1.73	2.29

can be attributed to reduced light scattering from the top of the micropillars, as due to the larger pitch, less micropillars are present per unit projected area. The optimum packing density is not known at this stage in our research.

The current densities were nevertheless lower than that of the previously presented device with random pyramid texture. Given the relatively large dimensions of the micropillars, we expect that further current density gains can be achieved by adding features with dimensions that are closer to or below the wavelength of light.

Furthermore, the length of the pillars could be increased to help the absorption. Elbersen et al. [10] showed the effect of pillar length on the J_{sc} of these structures. It was found that a length of 40 μm was optimum for light trapping in homojunction micropillar structures. However, increasing the length of the micropillars beyond 20 μm is challenging with the chosen deposition techniques, in particular the sputter technique for the ITO contact layer, which is highly anisotropic.

The V_{oc} of the micropillar devices was about ~20 mV lower than that of the flat reference. This is only a small decrease considering the increase of surface area and inevitably higher surface recombination that is introduced by the pillars. The fill factors of the devices with micropillars were higher than that of the flat reference cell, which is partly expressed by a lower series resistance in these devices. This could be an indication of more efficient carrier collection, caused by shorter collection paths of holes in the pillars.

In order to inspect the conformality of the different layers, coated pillars were cut in half along the z-direction using FIB milling and imaged by SEM as shown in Fig. 6. In this configuration, the single heterojunction is not visible in the SEM image. The ITO coating is clearly visible at the top of the micropillar in the SEM image. Due to the directionality of the sputtering technique used to deposit the ITO, an ITO thickness gradient is observed along the micropillar length. One way to better verify and visualize the composition along the height of the pillar is by energy selective backscattered (ESB) SEM imaging. ESB visualizes the contrast between the coating and the silicon micropillar and discriminates very accurately. The insets of Fig. 6 show that the ITO thickness changes from top to bottom, which is observed by the reduced ESB brightness along the length of the pillar from top to bottom. At the bottom the thickness of ITO is <10 nm and has a flaky structure. We expect that this change in thickness and composition is accompanied by a decrease of conductivity along the pillar. The latter limits the collection

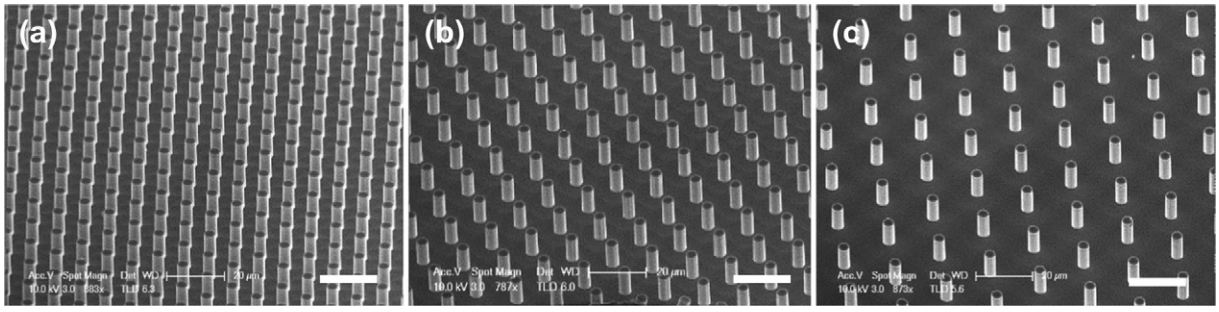

Fig. 5. Tilted SEM top view images of 20-μm long micropillars with different pitches: (a) 8 μm, (b) 10 μm and, (c) 15 μm. The scale bars are 20 μm.

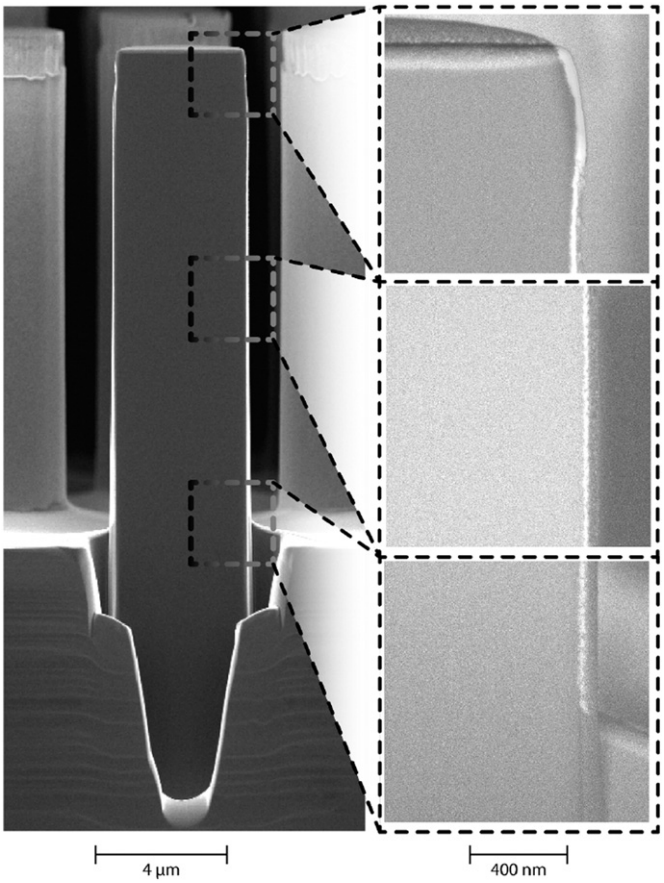

Fig. 6. Cross-sectional SEM images showing a micropillar of 20 µm that has been cut in half by FIB, orthogonally to the substrate, to be able to inspect the conformality of the different coatings along the pillar height. The insets are magnifications of the top, middle and bottom of the micropillar, in order to inspect the ITO layer.

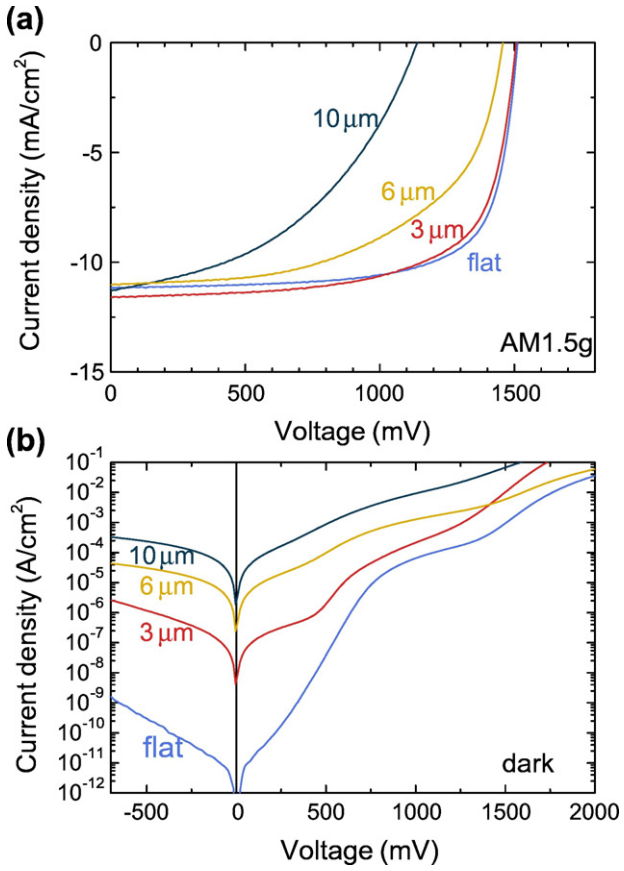

Fig. 7. Current density-voltage characteristics of a-Si:H/SHJ tandem solar cells with different micropillar lengths, under AM1.5G (a) and dark (b) conditions. The current densities under dark conditions are plotted on a logarithmic scale.

of the photogenerated charges. Increasing the length of the micropillar would only aggravate this problem. For this reason, we did not further increase the length of the micropillar. A more conformal deposition technique, such as atomic layer deposition [21] could be used in the future to reduce the thickness variation of the transparent metal oxide layer along the pillar length.

3.3. Micropillar a-Si:H/SHJ tandem cells

Micropillars arrays are one of the proposed geometries to use as photoelectrochemical cell in a solar to fuel device. However, many photoelectrochemical reactions, such as water splitting, require a higher operating voltage than that obtained with a single junction cell. To increase the operating voltage, we created a-Si:H n–i–p radial junctions on top of SHJ cells with a micropillar array. The obtained a-Si:H/SHJ n–i–p tandem structures basically resemble earlier so-called "honeymoon" tandem cells that have been fabricated with either diffused junction c-Si solar cells [22,23] or SHJ solar cells as bottom cells [16,24]. However, to our knowledge there are no earlier reports about these structures on micropillars. As absorber layer, a 350-nm thick a-Si:H intrinsic HWCVD layer was used. Although it is expected that this layer will not provide enough current to match that of the bottom SHJ cell, an increase in the thickness will likely result in a reduction of FF rather than a substantial increase of current density due to collection length limitations [25]. Therefore, we did not attempt to achieve current matching in this tandem cell.

Fig. 7(a) shows the *J–V* curves under AM1.5G conditions of representative tandem cells with various pillar lengths (with fixed spacing at ~15 µm) compared to a flat device, with Table 2 providing further details. Although all pillar lengths led to functional devices, the increase of pillar length caused a decrease of the FF and the V_{oc}. Due to the larger surface area of the micropillars, the dark current increases, which leads to a reduced V_{oc}. This decrease can also be understood when considering the *J–V* curves measured under dark conditions in Fig. 7(b). Even though it is not straightforward to derive a physical meaning from all aspects of the dark *J–V* curves of multijunction devices [26], the higher saturation currents that are observed for the longer pillar lengths are an indication of shunting paths in the top cells.

The performance of the flat and 3-µm micropillar device are significantly better than recent efforts on a-Si:H/SHJ tandem devices [16,24]. The V_{oc} of these cells is in good agreement with the sum of individual sub-cells (~650 mV for the SHJ and ~850 mV for the a-Si:H solar cell, adding up to ~1500 mV). EQE measurements showed that all devices were current-limited by the a-Si:H top cell, as expected. The pillar length did not have a large influence on the current densities that are generated by the top cells. Instead, a current density gain of the SHJ bottom cell was observed as the pillar length increases. This effect is most profound in the device with 10 µm pillars as shown in Fig. 8, where its EQE response is compared to that of a flat tandem solar cell. A similar

Table 2
Electrical characteristics of the a-Si:H/SHJ tandem solar cells. The spacing of the micropillars was ~15 µm.

Length (µm)	V_{oc} (mV)	J_{sc} (mA/cm^2)	FF (%)	η (%)	R_s (Ω·cm^2)	R_p (kΩ·cm^2)
Flat	1521	11.21	70.1	11.96	7.99	4.16
3	1507	11.59	67.6	11.81	7.27	2.92
6	1457	11.02	56.0	8.99	11.0	1.89
10	1139	11.29	44.1	5.67	25.8	0.38

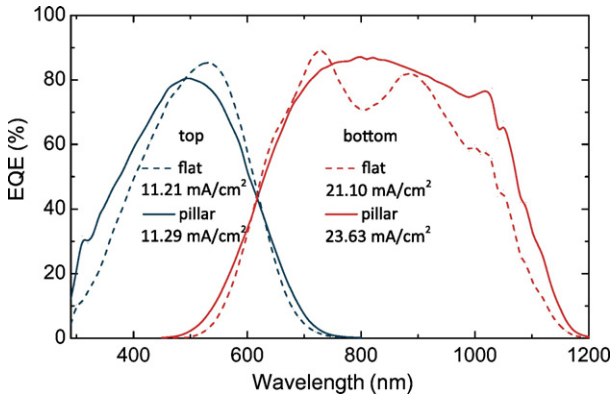

Fig. 8. External quantum efficiency of the a-Si:H/SHJ tandem solar cell with 10-μm long pillars (solid line) compared to that of a flat tandem (dashed line) under short circuit conditions. The response of the top and bottom cells were measured separately by applying infrared and blue bias LED illumination, respectively.

effect was observed in thin film silicon based tandem solar cells fabricated on a nanorod morphology [27]. The interference fringes caused by the optical contrast between c-Si and a-Si:H layers as seen in the flat device are almost absent in the pillar device due to enhanced absorption. The current gain in the bottom cell is not reflected in the *J–V* measurements due to unchanged current limitation by the top cell.

A micropillar with a length of 10 μm was cut in the z-direction by FIB milling in order to inspect conformality of the different deposited layers by SEM (see Fig. 9). The a-Si:H absorber layer is clearly visualized, due to the different morphology of the amorphous material from the crystalline silicon. A small difference in deposited thickness is visible between the top and side of the micropillar. Additionally, the layer thickness is gradually smaller along the micropillar length. This indicates a diffusion limitation of a-Si:H precursors during deposition.

3.4. Micropillar a-Si:H/a-SiGe:H/SHJ triple cells

To fabricate a fully integrated solar-to-fuel device, literature states a set of semiconductors must be combined with a proper electrocatalyst. Here, unbiased photoelectrolysis requires at least 1.23 V of photovoltage from semiconducting materials, without taking significant losses into account e.g. kinetic overpotentials needed to drive the hydrogen evolution and oxygen evolution reactions and mass-transport [28]. The best of our tandem devices, presented in the previous section, have a voltage at maximum power point (V_{mpp}) that barely exceeds this value. For this reason, we briefly explored the possibility of adding an extra junction in the device architecture. A 120-nm thick hydrogenated amorphous silicon germanium (a-SiGe:H) layer was added as a middle cell absorber of an a-Si:H/a-SiGe:H/SHJ triple junction device. The best results were obtained using a sample with micropillars which were 5 μm long, 4 μm in diameter, and had 4 μm spacing between them: V_{oc} = 1821 mV, J_{sc} = 6.14 mA/cm^2, FF = 65.6%, η = 7.33%. Although the current matching of this device is not optimized, the higher V_{mpp} (1472 mV) is better suited for photoelectrochemical water splitting, without the need of a bias voltage.

Fig. 10 shows a cross-sectional SEM image of a micropillar with an a-Si:H/a-SiGe:H/SHJ triple junction structure. The individual absorber layers are clearly visualized. Especially, the 120 nm of a-SiGe:H and 80 nm of ITO are bright in the SEM images. The top absorber of intrinsic a-Si:H is darker in color. For the intrinsic a-Si:H, a weak gradient in thickness is visible along the micropillar length. From the top to the bottom of the micropillar, the thickness of the a-Si:H layer gradually decreases in thickness. This is due a slight anisotropy in the deposition technique. This holds in a more pronounced way for the TRJs, which are deposited by PECVD. The TRJs are clearly visible on top of the c-Si micropillar and a-SiGe:H layer and at the bottom next to the micropillar. At the side of the micropillar this layer is hardly visible. The depletion of these layers is likely to be the reason for the poorer performance of the longer micropillars.

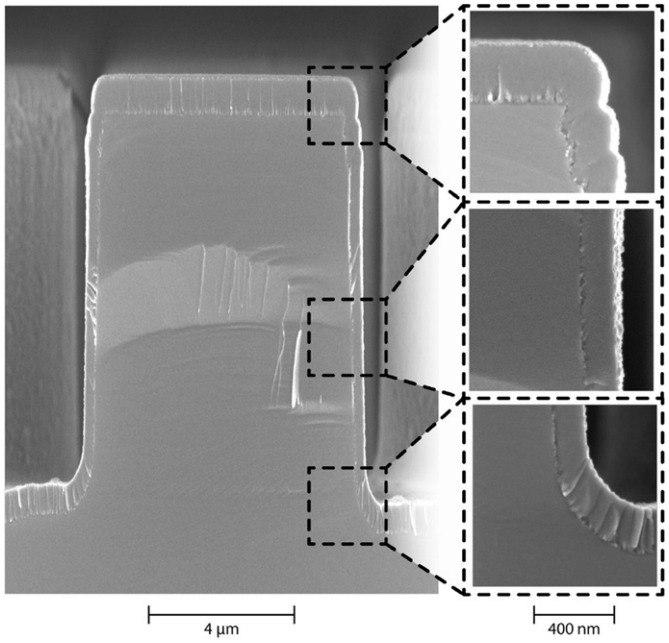

Fig. 9. Cross-sectional SEM images showing of 10 μm with a SHJ/a-Si:H tandem structure that has been cut in half by FIB. The insets are magnifications of the top, middle and bottom of the micropillar, in order to inspect the ITO layer.

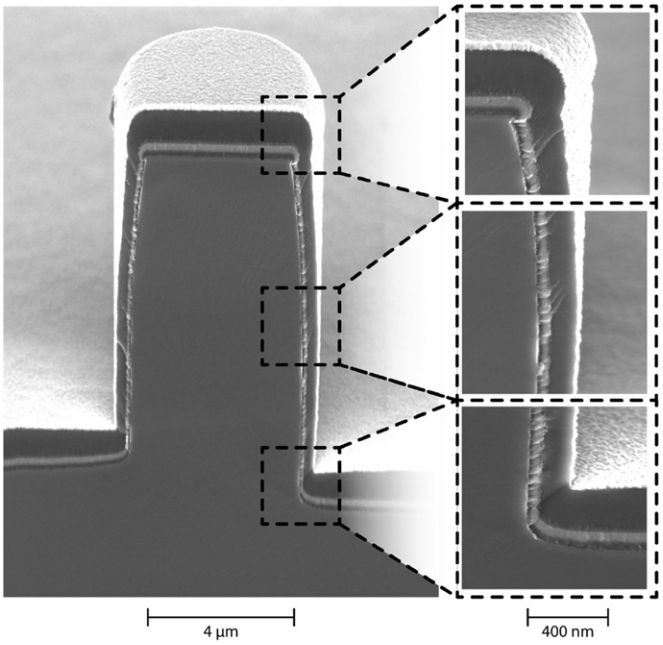

Fig. 10. Cross section of a micropillar solar cell with an a-Si:H/a-SiGe:H/SHJ triple junction structure. The insets show magnifications of the top, middle and lower part of the micropillar.

4. Conclusions

We have demonstrated the quality of hydrogenated amorphous silicon passivation layers deposited by hot wire chemical vapor deposition for silicon heterojunction solar cells with demanding surface morphologies. The high open-circuit voltages and 19.4% energy conversion efficiency on solar cells with a common random pyramid texture demonstrate the high quality of the passivation layer. The conformal nature of HWCVD avoids the need of post-texturization treatments to round off the sharp features in random pyramidal textures. This opens new avenues for the production of silicon heterojunction cells with thin intrinsic layers.

Utilizing the same conformal nature, we created radial heterojunctions on c-Si micropillar arrays with pillar heights of 20 μm, that show only limited loss of open-circuit voltage despite the vertical walls and the increase of surface area. For future use in photoelectrochemical fuel production devices, we fabricated multijunction solar cells with a silicon heterojunction as bottom cell and a-Si(Ge):H alloy n–i–p top cell(s), resulting in open-circuit voltages that are high enough for water splitting. The performance of a-Si:H/SHJ tandem cells was better than recent tandem structures of this type.

Acknowledgments

We thank Paula Bronsveld of ECN for supplying the random pyramid textured c-Si wafers and acknowledge NanoNextNL, a micro and nanotechnology consortium of the government of the Netherlands and 130 partners. This work is part of the research program of the Foundation for Fundamental Research on Matter (FOM, projects 115-10TBSC07-2 and 13CO12-2), which is part of the Netherlands Organization for Scientific Research (NWO).

References

[1] K. Masuko, M. Shigematsu, T. Hashiguchi, D. Fujishima, M. Kai, N. Yoshimura, T. Yamaguchi, Y. Ichihashi, T. Mishima, N. Matsubara, T. Yamanishi, T. Takahama, M. Taguchi, E. Maruyama, S. Okamoto, Achievement of more than 25% conversion efficiency with crystalline silicon heterojunction solar cell, IEEE J. Photovoltaics 4 (2014) 1433–1435, http://dx.doi.org/10.1109/jphotov.2014.2352151.

[2] F. Feldmann, M. Simon, M. Bivour, C. Reichel, M. Hermle, S.W. Glunz, Carrier-selective contacts for Si solar cells, Appl. Phys. Lett. 104 (2014) 181105, http://dx.doi.org/10.1063/1.4875904.

[3] D. Adachi, J.L. Hernández, K. Yamamoto, Impact of carrier recombination on fill factor for large area heterojunction crystalline silicon solar cell with 25.1% efficiency, Appl. Phys. Lett. 107 (2015) 233506, http://dx.doi.org/10.1063/1.4937224.

[4] C. Battaglia, A. Cuevas, S. De Wolf, High-efficiency crystalline silicon solar cells: status and perspectives, Energy Environ. Sci. 9 (2016) 1552–1576, http://dx.doi.org/10.1039/c5ee03380b.

[5] H. Umemoto, K. Ohara, D. Morita, Y. Nozaki, A. Masuda, H. Matsumura, Direct detection of H atoms in the catalytic chemical vapor deposition of the SiH_4/H_2 system, J. Appl. Phys. 91 (2002) 1650, http://dx.doi.org/10.1063/1.1428800.

[6] H. Matsumura, K. Higashimine, K. Koyama, K. Ohdaira, Comparison of crystalline-silicon/amorphous-silicon interface prepared by plasma enhanced chemical vapor deposition and catalytic chemical vapor deposition, J. Vac. Sci. Technol., B: Nanotechnol. Microelectron.: Mater., Process., Meas., Phenom. 33 (2015) 031201, http://dx.doi.org/10.1116/1.4915494.

[7] R.E.I. Schropp, Industrialization of hot wire chemical vapor deposition for thin film applications, Thin Solid Films 595 (2015) 272–283, http://dx.doi.org/10.1016/j.tsf.2015.07.054.

[8] M.D. Kelzenberg, S.W. Boettcher, J.A. Petykiewicz, D.B. Turner-Evans, M.C. Putnam, E.L. Warren, J.M. Spurgeon, R.M. Briggs, N.S. Lewis, H.A. Atwater, Enhanced absorption and carrier collection in Si wire arrays for photovoltaic applications, Nat. Mater. 9 (2010) 239–244, http://dx.doi.org/10.1038/nmat2635.

[9] M. Gharghi, E. Fathi, B. Kante, S. Sivoththaman, X. Zhang, Heterojunction silicon microwire solar cells, Nano Lett. 12 (2012) 6278–6282, http://dx.doi.org/10.1021/nl3033813.

[10] R. Elbersen, R.M. Tiggelaar, A. Milbrat, G. Mul, H. Gardeniers, J. Huskens, Controlled doping methods for radial p/n junctions in silicon, Adv. Energy Mater. 5 (2014) 1401745, http://dx.doi.org/10.1002/aenm.201401745.

[11] E.L. Warren, H.A. Atwater, N.S. Lewis, Silicon microwire arrays for solar energy-conversion applications, J. Phys. Chem. C 118 (2014) 747–759, http://dx.doi.org/10.1021/jp406280x.

[12] L.W. Veldhuizen, Y. Kuang, N.J. Bakker, C.H.M. van der Werf, S.J. Yun, R.E.I. Schropp, Hydrogenated amorphous silicon germanium by Hot Wire CVD as an alternative for microcrystalline silicon in tandem and triple junction solar cells, MRS Proc. 1666 (2014)http://dx.doi.org/10.1557/opl.2014.683.

[13] H.A. Gatz, J.K. Rath, M.A. Verheijen, W.M.M. Kessels, R.E.I. Schropp, Silicon heterojunction solar cell passivation in combination with nanocrystalline silicon oxide emitters, Phys. Status Solidi A (2016)http://dx.doi.org/10.1002/pssa.201532945.

[14] M. Edwards, S. Bowden, U. Das, M. Burrows, Effect of texturing and surface preparation on lifetime and cell performance in heterojunction silicon solar cells, Sol. Energy Mater. Sol. Cells 92 (2008) 1373–1377, http://dx.doi.org/10.1016/j.solmat.2008.05.011.

[15] L. Fesquet, S. Olibet, J. Damon-Lacoste, S. De Wolf, A. Hessler-Wyser, C. Monachon, C. Ballif, Modification of Textured Silicon Wafer Surface Morphology for Fabrication of Heterojunction Solar Cell With Open Circuit Voltage Over 700 mV, 2009 000754–000758, http://dx.doi.org/10.1109/pvsc.2009.5411173.

[16] Y. Lee, V.A. Dao, S.M. Iftiquar, S. Kim, J. Yi, Current transport studies of amorphous n/p junctions and its application in a-Si:H/HIT-type tandem cells, Prog. Photovolt. Res. Appl. 24 (2016) 52–58, http://dx.doi.org/10.1002/pip.2644.

[17] L.W. Veldhuizen, R.E.I. Schropp, Very thin and stable thin-film silicon alloy triple junction solar cells by hot wire chemical vapor deposition, Appl. Phys. Lett. 109 (2016) 093902, http://dx.doi.org/10.1063/1.4961937.

[18] L.W. Veldhuizen, C.H.M. van der Werf, Y. Kuang, N.J. Bakker, S.J. Yun, R.E.I. Schropp, Optimization of hydrogenated amorphous silicon germanium thin films and solar cells deposited by hot wire chemical vapor deposition, Thin Solid Films 595 (2015) 226–230, http://dx.doi.org/10.1016/j.tsf.2015.05.055.

[19] L. Schäfer, T. Harig, M. Höfer, A. Laukart, D. Borchert, S. Keipert-Colberg, J. Trube, In-line deposition of silicon-based films by hot-wire chemical vapor deposition, Surf. Coat. Technol. 215 (2013) 141–147, http://dx.doi.org/10.1016/j.surfcoat.2012.08.085.

[20] Q. Wang, M.R. Page, E. Iwaniczko, Y. Xu, L. Roybal, R. Bauer, B. To, H.C. Yuan, A. Duda, F. Hasoon, Y.F. Yan, D. Levi, D. Meier, H.M. Branz, T.H. Wang, Efficient heterojunction solar cells on p-type crystal silicon wafers, Appl. Phys. Lett. 96 (2010) 013507, http://dx.doi.org/10.1063/1.3284650.

[21] B. Macco, M.A. Verheijen, L.E. Black, B. Barcones, J. Melskens, W.M.M. Kessels, On the solid phase crystallization of In_2O_3:H transparent conductive oxide films prepared by atomic layer deposition, J. Appl. Phys. 120 (2016) 085314, http://dx.doi.org/10.1063/1.4962008.

[22] Y. Hamakawa, New types of high efficiency solar cells based on a-Si, Appl. Phys. Lett. 43 (1983) 644, http://dx.doi.org/10.1063/1.94462.

[23] K. Okuda, H. Okamoto, Y. Hamakawa, Amorphous Si/polycrystalline Si stacked solar cell having more than 12% conversion efficiency, Jpn. J. Appl. Phys. 22 (1983) L605–L607, http://dx.doi.org/10.1143/jjap.22.l605.

[24] T. Sameshima, J. Takenezawa, M. Hasumi, T. Koida, T. Kaneko, M. Karasawa, M. Kondo, Multi junction solar cells stacked with transparent and conductive adhesive, Jpn. J. Appl. Phys. 50 (2011) 052301, http://dx.doi.org/10.1143/jjap.50.052301.

[25] L.W. Veldhuizen, G.W.P. Adhyaksa, M. Theelen, E.C. Garnett, R.E.I. Schropp, Benchmarking Photoactive Thin-film Materials Using a Laser-induced Steady-state Photocarrier Grating, Prog. Photovolt.: Res. Appl. (2017) http://dx.doi.org/10.1002/pip.2889.

[26] A. Sturiale, H.T. Li, J.K. Rath, R.E.I. Schropp, F.A. Rubinelli, Exploring dark current voltage characteristics of micromorph silicon tandem cells with computer simulations, J. Appl. Phys. 106 (2009) 014502, http://dx.doi.org/10.1063/1.3151691.

[27] L.W. Veldhuizen, Y. Kuang, R.E.I. Schropp, Ultrathin tandem solar cells on nanorod morphology with 35-nm thick hydrogenated amorphous silicon germanium bottom cell absorber layer, Sol. Energy Mater. Sol. Cells (2016) http://dx.doi.org/10.1016/j.solmat.2016.03.041.

[28] M.G. Walter, E.L. Warren, J.R. McKone, S.W. Boettcher, Q. Mi, E.A. Santori, N.S. Lewis, Solar water splitting cells, Chem. Rev. 110 (2010) 6446–6473, http://dx.doi.org/10.1021/cr1002326.